

Two classes of fast-declining type Ia supernovae

Suhail Dhawan^{1,2,3}, B. Leibundgut^{1,2}, J. Spyromilio¹, and S. Blondin⁴

¹ European Southern Observatory, Karl-Schwarzschild-Strasse 2, D-85748 Garching bei München, Germany
e-mail: sdhawan@eso.org

² Excellence Cluster Universe, Technische Universität München, Boltzmannstrasse 2, D-85748, Garching, Germany

³ Physik Department, Technische Universität München, James-Frank-Strasse 1, D-85748 Garching bei München

⁴ Aix Marseille Université, CNRS, LAM, Laboratoire d'Astrophysique de Marseille, Marseille, France

Received; accepted

Abstract

Fast-declining Type Ia supernovae (SNIa) separate into two categories based on their bolometric and near-infrared (NIR) properties. The peak bolometric luminosity (L_{\max}), the phase of the first maximum relative to the optical, the NIR peak luminosity and the occurrence of a second maximum in the NIR distinguish a group of very faint SNIa. Fast-declining supernovae show a large range of peak bolometric luminosities (L_{\max} differing by up to a factor of ~ 8). All fast-declining SNIa with $L_{\max} < 0.3 \times 10^{43} \text{ erg s}^{-1}$ are spectroscopically classified as 91bg-like and show only a single NIR peak. SNe with $L_{\max} > 0.5 \times 10^{43} \text{ erg s}^{-1}$ appear to smoothly connect to normal SNIa. The total ejecta mass (M_{ej}) values for SNe with enough late time data are $\lesssim 1 M_{\odot}$, indicating a sub-Chandrasekhar mass progenitor for these SNe.

Key words. supernovae:general

1. Introduction

Type Ia supernovae have long been linked with the explosion of a C/O white dwarf (Hoyle & Fowler 1960). Ignition of the white dwarf can lead to fusion of (the) C/O to ^{56}Ni releasing enough energy to unbind the progenitor and through the deposition of the energy released in the radioactive decay of ^{56}Ni to ^{56}Co , and on to ^{56}Fe , power the electromagnetic display of the supernova. This scenario is extremely robust and is supported both by theoretical studies (Hillebrandt & Niemeyer 2000) and observations over many decades, although the exact white dwarf mass and ignition scenario remain the subject of extensive debate.

In the past two decades the study of supernovae has been blessed with an great increase in high quality data through a series of systematic surveys for transients and extended temporal and wavelength coverage. Dedicated supernova searches have discovered several SNIa with unusual photometric and spectroscopic properties. Some peculiar SNIa exhibit fast optical post-peak declines and a deep trough-like feature at $\sim 4200 \text{ \AA}$ in their maximum light spectra, attributed to TiII. The prototypical example of this class is SN 1991bg (Filippenko et al. 1992; Leibundgut et al. 1993; Mazzali et al. 1997). Li et al. (2011) showed that SN 1991bg-like events comprise a large fraction (15-20%) of the SNIa population in a volume-limited sample and appear distinct from normal SNIa in their width-luminosity relationship. SN 1991bg-like events have been shown to prefer elliptical and lenticular galaxies (Howell 2001).

Based on multi-epoch spectra and multi-band optical light curves of a sample of fast-declining, SN 1991bg-like SNIa, Taubenberger et al. (2008) suggested that this class may have a different physical origin to normal SNIa, although the possibility that they are a low-luminosity, fast-declining extension of normal SNIa cannot be excluded. These SNe show markedly different optical colour evolution and low ^{56}Ni mass values as calculated from UBVRI pseudo-bolometric light curves. Supernovae with intermediate properties between normal and sub-luminous SNIa would lend support to the latter hypothesis (Garnavich et al. 2004).

The optical width-luminosity relation for SNIa (Phillips et al. 1999; Burns et al. 2011) shows a notable break for fast-declining objects ($\Delta m_{15}(B) > 1.6$). Fast-declining SNIa are fainter given their $\Delta m_{15}(B)$ assuming a linear relation, possibly due to the inability of $\Delta m_{15}(B)$ to properly characterise fast-declining SNe since their light curves settle onto a linear magnitude decline at approximately 15 days past B maximum. Burns et al. (2014) proposed a different ordering parameter, s_{BV} , to improve the treatment of fast-declining objects. s_{BV} is defined as the epoch at which the $(B - V)$ colour curve is at its maximum value, divided by 30 d. Using this metric the fast-declining SNe appear less distinct and more as a continuous tail of the distribution of normal SNIa.

In the near infrared SNIa are remarkably uniform around maximum (Elias et al. 1981; Meikle 2000; Krisciunas et al. 2004; Folatelli et al. 2010; Dhawan et al. 2015). While a majority of SNIa show a homogeneous behaviour around the maximum, there are some clear out-

liers. Garnavich et al. (2004) reported that the 91bg-like SN 1999by was fainter in the NIR (*JHK* filters) than the average derived for normal SN Ia in Krisciunas et al. (2004). Subsequent studies found a bi-modality in the NIR light curve properties of fast-declining SN Ia (e.g. Krisciunas et al. 2009; Folatelli et al. 2010; Kattner et al. 2012; Phillips 2012). Events whose NIR primary maxima occur after *B*-band maximum ($t_B(\text{max})$) are sub-luminous in all bands compared to normal SN Ia. These sub-luminous SN Ia also tend to lack or have very weak second maxima in their NIR light curves. However, objects that peak in the NIR *before* $t_B(\text{max})$ have NIR absolute magnitudes comparable to normal SN Ia and show prominent (albeit, early) second maxima. Following these results, Hsiao et al. (2015) proposed the definition of ‘transitional’ SNe as fast-declining SN Ia with an NIR maximum before $t_B(\text{max})$.

In this paper we analyse the NIR and bolometric properties of fast-declining SN Ia to determine whether they are an extension of normal SN Ia or a distinct subclass. In section 2 we describe our sample and in section 3 we show that fast-declining SN Ia are found in two distinct groups. In sections 4.2 and 4.3 we examine other distinguishing characteristics of the groups. The discussion and conclusions are presented in sections 5.

2. Data

We compiled a sample of fast-declining SN Ia with $\Delta m_{15} > 1.6$ from the literature. We do not include objects similar to 2002cx (dubbed ‘Type Iax’ supernovae Foley et al. 2013). Some of Iax SNe are fast decliners (e.g. SN 2002cx, Li et al. 2003; SN 2005hk, Jha et al. 2006; Phillips et al. 2007; SN 2008ha, Foley et al. 2009) and could have been included in our sample, but the evidence for them being different kinds of explosions is mounting (e.g. Li et al. 2003; Jha et al. 2006). We discuss some of the SNIax features in the conclusions.

Most of our data is compiled from the Carnegie Supernova Project (CSP; Contreras et al. 2010; Stritzinger et al. 2011) augmented by the CfA supernova survey on PAIRITEL (Wood-Vasey et al. 2008; Friedman et al. 2015). To these objects we add SN 1999by (Garnavich et al. 2004) and iPTF13ebh (Hsiao et al. 2015). The objects in our sample along with the sources of the data are presented in Table 1.

Our sample has 15 SNe. Ten of these SNe are spectroscopically classified as 91bg-like (Garnavich et al. 2004; Folatelli et al. 2013). Seven SNe in our sample show a pronounced NIR second maximum, three of which are spectroscopically 91bg-like (2006gt, 2007ba and 2008R).

For SNe with $z > 0.01$, we use luminosity distances with $H_0 = 70 \text{ km s}^{-1} \text{Mpc}^{-1}$, $\Omega_m = 0.27$ and $\Omega_\Lambda = 0.73$. For nearby SNe with $z < 0.01$ we use independent distances to the host galaxy from the literature. A summary of the methods used for the distances and the references is provided in Table 1.

For SNe observed by the CSP, we have used published values of s_{BV} . For other SNe we calculated the s_{BV} from SNooPY (Burns et al. 2011) fits to the data.

3. Luminosity vs colour-stretch: Evidence for two classes of fast-declining SNe

As has been discussed in Dhawan et al. (2015) the infrared spectral region (*JHK*) is a significant contributor to the bolometric luminosity of SN Ia. We calculate the pseudo-bolometric light curve by integrating over a $u \rightarrow H$ (UVOIR) SED based on monochromatic fluxes derived using the transmission curves for each survey (see Contardo, Leibundgut & Vacca 2000, for a detailed explanation of the method). The light curves are corrected for host galaxy and Milky Way extinction. We determine the absolute UVOIR peak luminosity (L_{max}) by fitting a cubic spline to the constructed pseudo-bolometric light curve.

The s_{BV} versus L_{max} relationship (Figure 1) exhibits two distinct groups among the fast declining SN Ia. One group extends the trend of normal Ia supernovae with lower luminosity having an earlier s_{BV} while a second group is detached and appears to follow a different relation. The relation for the faint subgroup has a significantly different slope ($\sim 2\sigma$ level; Table 2). We note that the error in the slope for fitting all SNe as single group is lower than the two separate subgroups. However, this is because the total sample size is greater than the comparatively smaller subsamples of the two separate groups.

A simple χ^2/DoF analysis shows that a fit to two subclasses (fitting two slopes simultaneously) is favoured (reduced $\chi^2 = 1.03$ compared to a single line fit (reduced $\chi^2 = 1.90$). We also apply the hypothesis testing technique of comparing the logarithm of the Bayesian Evidence ($\ln Z$; see Skilling 2004, for details about). Z is the integral of the likelihood over the prior region

$$Z = \int L \pi d\theta \quad (1)$$

where L is the likelihood, π is the prior and θ is the set of the parameters. We calculate $\ln Z$ using a multi-modal nested sampling algorithm, MultiNest (Feroz et al. 2013). The $\Delta \ln Z$ for the single population relative to the two subclasses is ~ -6.97 suggesting a strong preference for the two subclasses over the single population (Trotta 2008, suggest that $\Delta \ln Z < -5$ is strong evidence for the alternate model over null hypothesis).

This is an intriguing result suggesting that there are two separate populations of fast-declining SN Ia which we refer to as *SNIa-faint* here, as opposed the group that appears to join the normal SN Ia. The fainter group consists of SNe 1999by, 2005ke, 2006mr, 2007N, 2007ax and 2009F.

We note that Burns et al. (2014, their Fig. 10) find a the relation between the pseudo equivalent width of the Si II 5972 Å line and s_{BV} , which has a more complicated form than a simple linear relation for SNe with $s_{BV} < 0.5$. This would be further evidence that the *SNIa-faint* group of fast-declining SN Ia are a separate population.

4. Characterising fast-declining, low-luminosity SN Ia

There appear to be at least three distinguishing characteristics of the *SNIa-faint* subgroup. In addition to their extreme low luminosity, they appear to reach the NIR peak at a later stage compared to optical wavelengths and do not show a second maximum in their near-infrared light curves.

Table 1. SN sample used in this analysis.

SN	$t_B(max)$ (MJD; d)	$\Delta m_{15}(B)$ (mag)	s_{BV}	s_{BV} Reference (d)	$t_2(Y)$ ¹ (d)	$t_2(J)$ (mag)	μ	Distance Method **	Distance Reference	Data Reference
<i>SN1999bg</i> ^{*2}	51308.3	1.93	0.46	This paper	N/A	N/A	30.82 (± 0.15)	TF	T13	H02,G04
SN2003gs	52848.3	1.83	0.49	This paper	...	15.3 (± 0.7)	31.65 (± 0.28)	SBF	T01	K09
<i>SN2005bl</i> [*]	53481.6	1.80	0.39	B14	N/A	N/A	35.14 (± 0.09)	LD		WV08, F15
<i>SN2005ke</i> [*]	53698.6	1.78	0.41	B14	N/A	...	31.84 (± 0.08)	SBF	T01	WV08, C10, F15
SN2006gt [*]	54003.1	1.66	0.56	B14	...	20.2 (± 1.2)	36.43 (± 0.05)	LD		C10
<i>SN2006mr</i> [*]	54050.2	1.84	0.26	B14	N/A	N/A	31.15 (± 0.23)	SBF	A01	C10
<i>SN2007N</i> [*]	54124.3	1.79	0.29	B14	N/A	N/A	33.91 (± 0.16)	LD		S11
<i>SN2007ax</i> [*]	54187.5	1.86	0.36	B14	N/A	N/A	32.20 (± 0.14)	TF	T09	S11
SN2007ba [*]	54196.2	1.88	0.54	B14	20.0 (± 0.4)	...	36.18 (± 0.05)	LD		S11
SN2007on	54421.1	1.90	0.57	B14	18.7 (± 0.4)	18.2 (± 0.1)	31.45 (± 0.08)	SBF	J03	S11
SN2008R [*]	54494.3	1.85	0.59	B14	15.5 (± 0.7)	14.1 (± 0.7)	33.73 (± 0.16)	LD		S11
SN2008hs	54812.1	1.83	0.60	This paper	...	14.0 (± 1.0)	34.28 (± 0.13)	LD		F15
<i>SN2009F</i> [*]	54841.8	1.97	0.33	B14	N/A	N/A	33.73 (± 0.16)	LD		S11
SN2010Y	55247.5	1.73	0.61	This paper	33.44 (± 0.20)	LD		F15
iPTF13ebh	56622.9	1.79	0.63	H15	19.4 (± 0.2)	17.2 (± 1.5)	33.63 (± 0.16)	LD		H15

Notes. ⁽¹⁾ SN Ia with only one maximum are marked as ‘N/A’. Ellipses indicate insufficient data to determine a second maximum.

⁽²⁾ SN Ia in the *SN Ia-faint* group are shown in *italics* (see text)

(*) Spectroscopically classified as SN 1991bg-like

(**) Methods for distances to the SN hosts are as follows: LD: luminosity distance (using parameters detailed in the text), TF: Tully-Fisher relation, SBF: surface brightness fluctuation. Note that 0.16 mag (Jensen et al. 2003) is subtracted from SBF distances from Tonry et al. (2001) to put them on the same scale as Freedman et al. (2001). Note that objects that do not have a luminosity distance presented here are not in the Hubble flow i.e. have $z < 0.01$.

References. A01: Ajhar et al. (2001), T01: Tonry et al. (2001), H02: Höflich et al. (2002), J03: Jensen et al. (2003), G04: Garnavich et al. (2004), K09: Krisciunas et al. (2009), WV08: Wood-Vasey et al. (2008), C10: Contreras et al. (2010), S11: Stritzinger et al. (2011), T09: Tully et al. (2009), T13: Tully et al. (2013), F15: Friedman et al. (2015), H15: Hsiao et al. (2015)

Table 2. Slope and intercept for the $L_{max} - s_{BV}$ relation

Sample	Slope	Intercept
<i>SN Ia-faint</i>	0.76 (± 0.17)	-0.08 (± 0.06)
Normal SN Ia	1.24 (± 0.14)	-0.05 (± 0.11)
Complete	1.40 (± 0.08)	-0.27 (± 0.04)

4.1. Phase of the first NIR maximum

As originally pointed out by Contardo, Leibundgut & Vacca (2000) and extended by future studies (Krisciunas et al. 2004; Kattner et al. 2012; Dhawan et al. 2015) regular SN Ia reach the first maximum in the infrared several days earlier than in the optical bands. The physical reason for this is not entirely obvious, but could be due to the rapid shift of the SED to the blue as the spectrum-formation region heats up (Blondin, Dessart, & Hillier 2015). Several low-luminosity SN Ia reach their NIR peaks after the optical maximum (Krisciunas et al. 2004; Kattner et al. 2012). We have investigated this for our sample. The magnitude and epoch of the NIR maximum for our sample is reported in Table 3 and displayed against the bolometric peak luminosity in Fig. 2. The separation between the two groups is a function of wavelength and appears to increase from Y to H , with the effect being evident in J and H and less visible in Y . Similar to Fig. 1 the luminosity appears to be the distinguishing property, while the timing of the NIR maximum wrt $t_B(max)$ seems more like a continuous distribution. Nevertheless, the objects in our *SN Ia-faint* are separated from the normal SN Ia. We also note that these objects are also sub-luminous in the NIR filters, whereas SNe which peak before $t_B(max)$ are *not sub-luminous*.

4.2. Lack of NIR second maximum

A further characteristic property of *SN Ia-faint* is a lack of a second infrared maximum. Table 1 indicates the phase of the second maximum when it could be measured. Objects without a second maximum are labelled ‘N/A’ and correspond to the low-luminosity objects. There is a clear separation of the class of *SN Ia-faint* in this respect. We cannot confirm the UV to NIR (UVOIR) luminosity of SN 2005bl independently, but the lack of a second maximum, the late phase of the first maximum and low s_{BV} , indicate that this object also belongs to the *SN Ia-faint* subgroup¹.

4.3. Low ^{56}Ni and ejecta mass

We can further investigate the properties of fast-declining SN Ia by calculating the ejecta masses and production of ^{56}Ni .

From our calculated L_{max} , we estimate the ^{56}Ni mass using:

$$L_{max} = 2.0(\pm 0.3) \times 10^{43} \frac{M_{^{56}\text{Ni}}}{M_{\odot}} \text{ergs}^{-1}. \quad (2)$$

This is a simple implementation of Arnett’s rule (Arnett 1982; Arnett et al. 1985) for a rise time of 19 days. Variations in Arnett’s rule have been encapsulated in a parameter α (see Branch 1992). We use $\alpha = 1$. Taubenberger et al. (2008) find that fast-declining SN Ia have shorter rise times (typically 13 -16d) which would imply lower ^{56}Ni masses by 40-15 % for the same L_{max} . The resulting ^{56}Ni masses for 13 and 19 days rise times are reported in Table 4.

Unsurprisingly, the values of ^{56}Ni mass in Table 4 are significantly lower than the averages derived for normal

¹ Moreover, a low ^{56}Ni mass ($\sim 0.1 M_{\odot}$) from UBVRI light curve calculations by Taubenberger et al. (2008) lends further evidence to its classification as *SN Ia-faint*

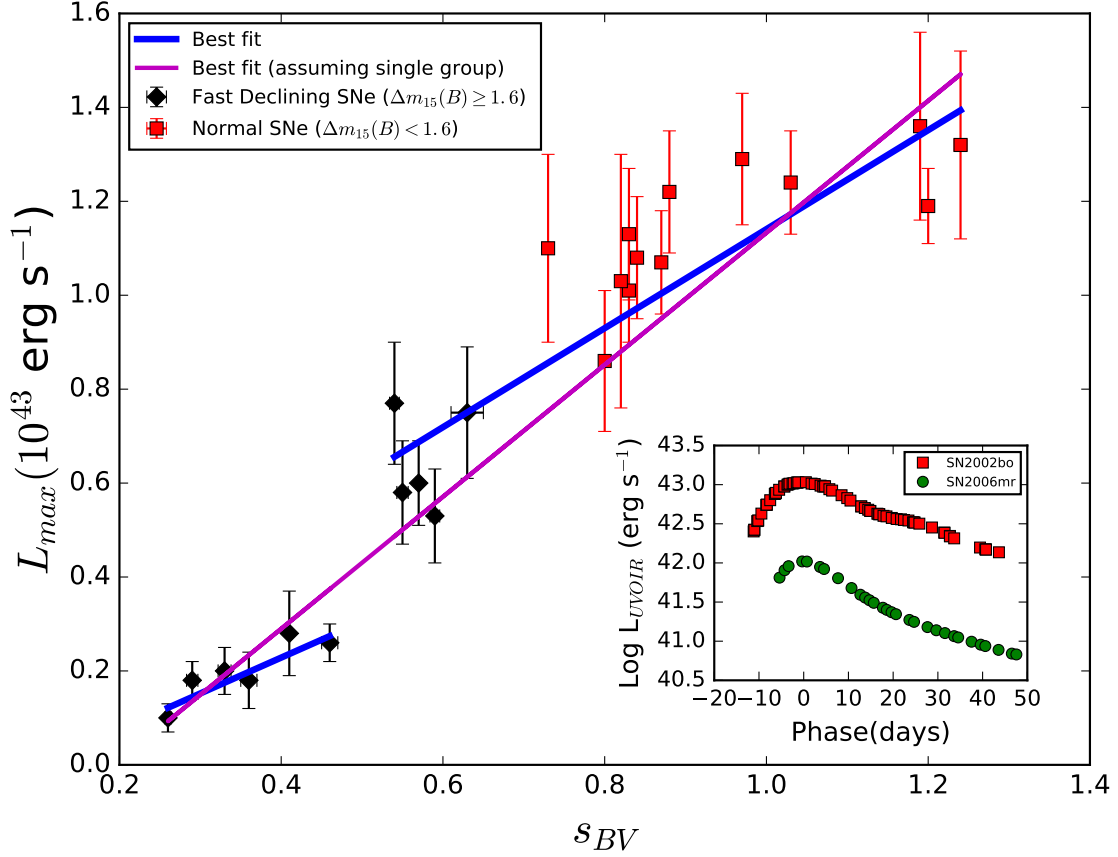


Figure 1. L_{\max} versus s_{BV} for normal SNIa (red) and fast-declining SNIa (black). The best fit linear relations for the faint sub-group of the fast-declining SNIa, the normal SNe, as well as the best fit assuming that all SNe belong to the same group are plotted as solid lines. The L_{\max} values for the normal SNIa were calculated in Dhawan et al. (2016) and the s_{BV} values are from Burns et al. (2014). *Inset:* The $u \rightarrow H$ pseudo-bolometric light curve for SN 2006mr (*green*), the faintest SN in the sample is plotted in comparison with the normal SN 2002bo (*red*; Benetti et al. 2004). From the bolometric light curves it is clear that SN 2006mr has a faster post-maximum evolution and settles earlier onto the exponential tail than SN 2002bo which was well described by a M_{Ch} delayed detonation model (Benetti et al. 2004; Blondin, Dessart, & Hillier 2015). The reduced χ^2 for the single population is 1.90 whereas for the two subclasses is 1.03

SNIa ($0.5 - 0.6 M_{\odot}$; e.g. Stritzinger et al. 2006; Scalzo et al. 2014; Dhawan et al. 2016). The ^{56}Ni mass values we derive range from $0.05 - 0.38 M_{\odot}$ indicating a significant diversity in the sample. A basic assumption in equation 2 is that the ejecta mass is the same for all SNIa when determining a nickel mass. If the *SNIa-faint* have a lower ejecta mass then the derived nickel masses estimates presented here are too large (Pinto & Eastman 2000). Of course equation 2 does not apply if other processes than photon diffusion or a different energy source are at work in low-luminosity SNIa. We allow the rise to vary between 13 and 19 days in our derivation of the ^{56}Ni mass. The results are presented in Tab. 4.

To calculate the ejecta mass we use (see Jeffery 1999, for a detailed derivation):

$$M_{ej} = 1.38 \cdot \left(\frac{1/3}{q}\right) \cdot \left(\frac{v_e}{3000 \text{ km s}^{-1}}\right)^2 \cdot \left(\frac{t_0}{36.80 \text{ d}}\right)^2 M_{\odot} \quad (3)$$

Equation 3 encapsulates the capture rate of γ -rays in an expanding spherical volume for a given distribution of the radioactive source. The e-folding velocity v_e provides the scal-

ing length for the expansion, q is a qualitative description of the distribution of the material within the ejecta with $1/3$ being a uniform distribution and higher values reflecting more centrally concentrated ^{56}Ni . We assume a constant γ ray opacity of $0.025 \text{ cm}^2 \text{ g}^{-1}$ (Swartz, Sutherland, & Harkness 1995).

The ‘fiducial’ timescale (t_0) defined by Jeffery (1999) as a parameter that governs the time-varying γ -ray optical depth behaviour of a supernova is the only ‘observable’.

We determine t_0 by fitting the radioactive decay energy deposition to the late time (40–90 days) bolometric light curve (see Equation 4). As the UVOIR light curve is not truly bolometric there is an implicit assumption that the thermal infrared and the ultraviolet beyond the atmospheric cut off are not significant contributors. This assumption is supported by modelling that shows that the infrared catastrophe does not occur until much later and the line blanketing opacity in the UV remains high (Blondin, Dessart, & Hillier 2015; Fransson & Jerkstrand 2015). The deposition function for re-processed photons is then given by the following equation:

Table 3. Epoch of maximum (with respect to $t_B(\text{max})$) and peak magnitude in $YJHK$ filters

SN ¹	t_Y (d)	t_J (d)	t_H (d)	M_Y (mag)	M_J (mag)	M_H (mag)
<i>1999by</i>	2.98 (± 0.63)	-18.33 (± 0.19)
<i>2005bl</i>	...	1.12 (± 1.09)	-17.96 (± 0.13)	...
<i>2005ke</i>	1.88 (± 0.52)	1.33 (± 0.23)	2.05 (± 0.28)	-17.42 (± 0.08)	-17.45 (± 0.08)	-17.50 (± 0.08)
<i>2006mr</i>	5.46 (± 0.41)	3.26 (± 0.12)	5.11 (± 0.47)	-17.17 (± 0.23)	-17.17 (± 0.23)	-17.27 (± 0.23)
<i>2007N</i>	6.62 (± 1.03)	4.92 (± 2.00)	5.96 (± 1.30)	-17.48 (± 0.16)	-17.48 (± 0.18)	-17.65 (± 0.21)
<i>2007ax</i>	5.56 (± 0.24)	...	4.41 (± 1.63)	-17.01 (± 0.14)	...	-17.00 (± 0.15)
<i>2007ba</i>	1.12 (± 0.63)	-1.05 (± 1.9)	-0.42 (± 1.40)	-18.65 (± 0.06)	-18.56 (± 0.31)	-18.64 (± 0.11)
<i>2007on</i>	-2.88 (± 0.10)	-2.67 (± 0.10)	-3.49 (± 0.10)	-18.28 (± 0.19)	-18.37 (± 0.19)	-18.18 (± 0.19)
<i>2008hs</i>	...	-2.77 (± 0.63)	-3.21 (± 1.69)	...	-17.96 (± 0.15)	-17.82 (± 0.15)
<i>2009F</i>	5.14 (± 0.90)	1.80 (± 1.00)	...	-17.64 (± 0.19)	-17.57 (± 0.17)	...
<i>2010Y</i>	...	-1.88 (± 1.70)	-18.21 (± 0.26)	...
iPTF13ebh	-2.02 (± 0.10)	-0.48 (± 0.09)	-2.62 (± 0.91)	-18.57 (± 0.16)	-18.58 (± 0.16)	-18.46 (± 0.16)

Notes. ⁽¹⁾ SN Ia in the *SN Ia-faint* group are shown in *italics*

Table 4. ⁵⁶Ni masses for fast-declining SN Ia with sufficient early time coverage to determine a peak luminosity

SN ¹	L_{max} (10^{43} erg s ⁻¹)	M_{56Ni} $t_R=13$ d; M_\odot	M_{56Ni} $t_R=19$ d; M_\odot	$E(B-V)_{host}$ mag	$E(B-V)_{MW}$ mag	R_V^2	Reference for $E(B-V)_{host}$
<i>1999by</i>	0.26 (± 0.04)	0.10 (± 0.02)	0.13 (± 0.03)	0.020 (± 0.030)	0.010	3.1	G04
<i>2005ke</i>	0.28 (± 0.09)	0.10 (± 0.04)	0.14 (± 0.04)	0.263 (± 0.033)	0.020	1.0	B14
<i>2006gt</i>	0.58 (± 0.11)	0.21 (± 0.05)	0.29 (± 0.07)	0.040 (± 0.014)	0.032	3.1	B14
<i>2006mr</i>	0.10 (± 0.03)	0.04 (± 0.01)	0.05 (± 0.02)	0.089 (± 0.039)	0.018	2.9	B14
<i>2007N</i>	0.18 (± 0.04)	0.07 (± 0.02)	0.09 (± 0.03)	0.350 (± 0.052)	0.034	1.7	B14
<i>2007ax</i>	0.17 (± 0.06)	0.07 (± 0.02)	0.09 (± 0.03)	0.213 (± 0.049)	0.045	2.1	B14
<i>2007ba</i>	0.77 (± 0.13)	0.28 (± 0.06)	0.38 (± 0.09)	0.150 (± 0.026)	0.032	1.1	B14
<i>2007on</i>	0.60 (± 0.09)	0.22 (± 0.05)	0.30 (± 0.07)	<0.007	0.010	1.9	B14
<i>2008R</i>	0.53 (± 0.10)	0.20 (± 0.05)	0.27 (± 0.07)	0.009 (± 0.013)	0.062	3.1	B14
<i>2009F</i>	0.20 (± 0.05)	0.07 (± 0.02)	0.10 (± 0.03)	0.108 (± 0.047)	0.089	1.0	B14
iPTF13ebh	0.75 (± 0.14)	0.28 (± 0.07)	0.38 (± 0.10)	0.050 (± 0.020)	0.067	3.1	H15

Notes. ⁽¹⁾ SN Ia in the *SN Ia-faint* group are shown in *italics*

Notes. ⁽²⁾ R_V values were calculated using SNooPY fits (Burns et al. 2011, 2014).

References. G04: Garnavich et al. (2004), B14: Burns et al. (2014), H15: Hsiao et al. (2015)

$$E_{dep} = E_{Ni} + E_{Co,e^+} + [1 - \exp(-\tau)] \cdot E_{Co,\gamma} \quad (4)$$

Among the fast-declining SN Ia we have 5 objects for which we can determine both the maximum bolometric luminosity and the fiducial decay time scale, and hence, can derive both M_{ej} and M_{56Ni} . As described above, the application of Arnett's rule implicitly assumes an ejecta mass through its impact on the diffusion timescale. The rise time of the bolometric light curve is governed by a combination of M_{56Ni} and M_{ej} and as noted earlier attempted to capture any uncertainties in this combination by adopting two rise times for the calculation (13 and 19 days). These rise times have been consistently applied also to the determination of M_{ej} . In addition, the fiducial time scale depends on the density structure of the ejecta, which may differ for the fast-declining SN Ia and we explored two different e-folding velocities (2700 km s⁻¹ and 3000 km s⁻¹) to represent the range of possible ejecta structures. The least luminous delayed detonation models of Blondin et al. (2013) had a density profile well characterised by an e-folding velocity of 2500 km s⁻¹ while the typical value for more luminous models was close to 3000 km s⁻¹ (which is similar to the typical e-folding velocity for the sub- M_{Ch} models of Sim et al. (2010)). The results are presented in Table 5. We take

the range of results to define the uncertainty in our determination of the ejecta mass. The observational error contribution is negligible by comparison. For our analysis, we use $\alpha=1$. Recent theoretical studies (e.g. Blondin et al. 2013, 2016) find α to be within 20% of unity. Even for $\alpha = 1.2$, we would obtain a longer transparency timescale, t_0 by $\sim 15\%$. However, the high values of α imply a more centrally concentrated ⁵⁶Ni distribution and hence, a higher value for q . Moreover, the high α values correspond to the least luminous models (e.g. Blondin et al. 2013). For SNe corresponding to these luminosities, there is independent evidence for a central concentration of ⁵⁶Ni (for e.g. from low iron line widths in nebular spectra; for e.g., see Blondin et al. 2012) which would imply a significantly higher q value than assumed here ($q=1$ compared to $q=1/3$ used here), hence, counterbalancing the effect of a higher α (see Equation 3)

The derived M_{ej} of the *SN Ia-faint* are a clear indication that these are sub-Chandrasekhar explosions. The highest M_{ej} are found for the shortest rise times and the highest e-folding velocity, i.e. the shallowest density structure.

Combining Tables 4 and 5 (for a rise time of 13 days), we calculate the ratio of the M_{ej} to M_{56Ni} (hereafter, R_M) for fast-declining SN Ia. Fast-declining SN Ia in the *SN Ia-faint* sub-group have significantly larger R_M values compared to normal SN Ia (Figure 3). An interesting object is

Table 5. Fiducial time scales (t_0), ejecta masses (M_{ej}) and bolometric decline rate for the low-luminosity SN Ia with sufficient early and late time coverage to determine a peak luminosity and a late time slope (see text for assumptions about v_e , κ , and q).

SN	t_0 ($t_R = 13$ d) (d)	t_0 ($t_R = 19$ d) (d)	M_{ej} ($t_R=13$ d) (M_\odot ; $v_e=3000$ km s $^{-1}$)	M_{ej} ($t_R=13$ d) (M_\odot ; $v_e=2700$ km s $^{-1}$)	M_{ej} ($t_R=19$ d) (M_\odot ; $v_e=3000$ km s $^{-1}$)	M_{ej} ($t_R=19$ d) (M_\odot ; $v_e=2700$ km s $^{-1}$)	Decline rate (mag d $^{-1}$)
2005ke	31.69 (± 0.83)	28.49 (± 0.60)	1.03 (± 0.24)	0.84 (± 0.20)	0.83 (± 0.20)	0.67 (± 0.16)	0.030 (± 0.0004)
2006mr	26.72 (± 0.47)	24.67 (± 0.40)	0.73 (± 0.19)	0.61 (± 0.17)	0.62 (± 0.17)	0.51 (± 0.16)	0.039 (± 0.0013)
2007ax ¹	28.27 (± 0.69)	26.07 (± 0.50)	0.81 (± 0.21)	0.70 (± 0.18)	0.70 (± 0.18)	0.56 (± 0.16)	...
2007on	29.70 (± 0.77)	26.89 (± 0.16)	0.90 (± 0.21)	0.72 (± 0.19)	0.74 (± 0.19)	0.60 (± 0.16)	0.033 (± 0.0003)
2009F ¹	26.49 (± 0.60)	24.69 (± 0.40)	0.72 (± 0.19)	0.60 (± 0.16)	0.62 (± 0.16)	0.51 (± 0.14)	...

Notes. ⁽¹⁾ Only using UBVRI data

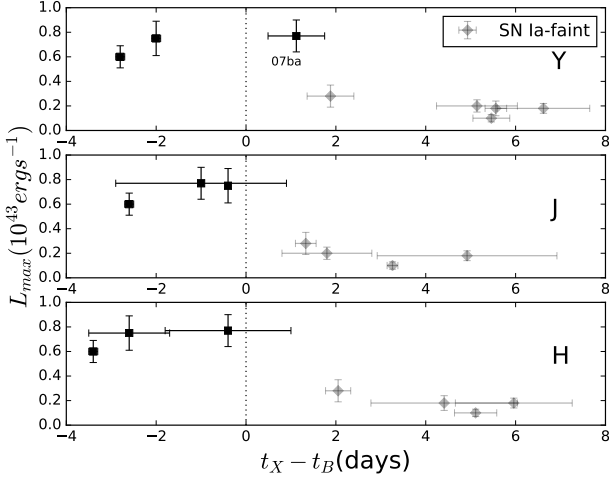


Figure 2. The pseudo-bolometric peak luminosity versus the timing of the NIR (YJH filters) maximum for SNe in our sample. SNe that peak *earlier* in the NIR (*squares*) than the optical also appear to be an extension to the normal SN Ia whereas all SNe with an NIR peak *after* the optical (*diamonds*) appear to be a distinct population in Figure 1. We note that in the Y -band there is one exception, SN 2007ba which has a high bolometric peak luminosity but a Y -band first maximum shortly *after* $t_B(\max)$

SN 2007on, which is the only fast-declining SN Ia connected to the normal SN Ia, and displays a $R_M = 4.5$ and is much closer to the value of normal SN Ia with $R_M < 4$. We also show in Figure 3 the values from different explosion models. The observed ratios of the *SN Ia-faint* agree better with sub- M_{Ch} model values than with the M_{Ch} values, although the errors are large due to large uncertainties in the individual M_{ej} and M_{56Ni} values.

For longer rise times the derived M_{ej} decrease and the M_{56Ni} estimates increase, which leads to small R_M . In this case, the points tend to drop further below the line of M_{Ch} explosions.

5. Discussion and Conclusion

The ejecta-mass estimates for our SN sample (Table 5) suggests that fast-declining SN Ia are associated with sub- M_{Ch} progenitors. Pure detonations of sub- M_{Ch} WDs have also been shown to compare favourably with the narrow light curves of low-luminosity SN Ia and hence reproduce the faint end of the width-luminosity relation (Sim et al. 2010; Blondin 2015; Blondin et al. 2016). One possible

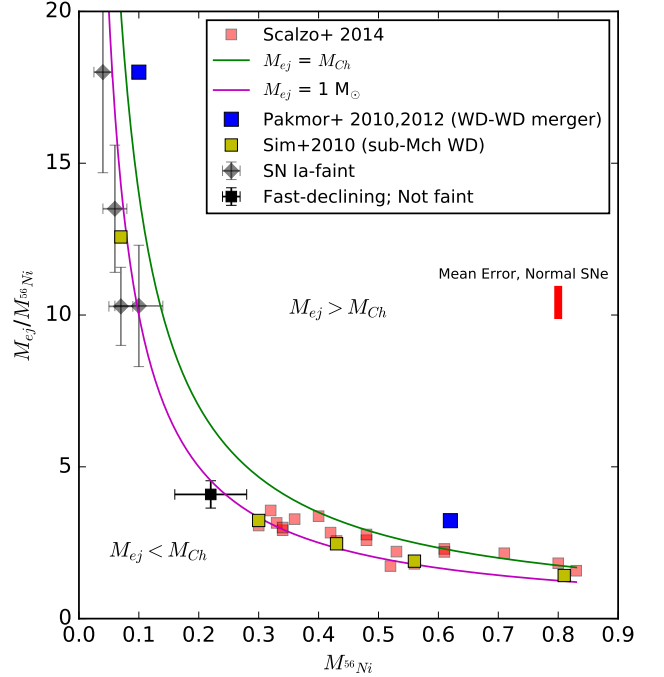


Figure 3. The ratio of the ejecta mass to ^{56}Ni mass is plotted against the ^{56}Ni mass. With decreasing ejecta mass the black points are SNe 2005ke, 2006mr, 2007on 2007ax and 2009F, the last two of which lack NIR coverage. The diamonds are the *SN Ia-faint* subgroup and the square is 2007on which is fast-declining but not in the subgroup. The red points are normal SN Ia taken from Scalzo et al. (2014). We also plot the values from different model scenarios. The yellow squares are sub- M_{Ch} double detonation models from Sim et al. (2010), blue squares from violent merger models for normal and subluminous SNe from Pakmor et al. (2010, 2012), the green curve is the ratio for a M_{Ch} explosion and the magenta curve is the ratio for a sub- M_{Ch} explosion with M_{ej} of $1 M_\odot$. We plot the typical error bar for the normal SNe from Scalzo et al. (2014) in red.

mechanism to trigger a sub- M_{Ch} WD explosion is the detonation of a surface layer of He, accreted from a companion (e.g. Bildsten et al. 2007), which in turn triggers a secondary carbon detonation in the WD core (known as the double detonation scenario Woosley & Weaver 1994; Livne & Arnett 1995; Fink et al. 2010; Shen & Moore 2014).

Two SNe in the *SN Ia-faint* subgroup (SN 1999by and SN 2005ke) show significantly larger continuum polarisation

(Howell 2001; Patat et al. 2012) than normal SNIa (e.g. see Wang et al. 2007; Patat et al. 2009). Detailed modelling of the polarisation spectra of SN 2005ke (Patat et al. 2012) led to the conclusion that it could arise from one of three scenarios; a WD rotating at close to break-up velocity, a M_{Ch} delayed detonation or a merger of two WDs. A significantly sub- M_{Ch} ejecta mass (Table 5) combined with the conclusions from the polarimetry would suggest a merger of two WDs (with total mass $M_{\text{tot}} < M_{\text{Ch}}$; see van Kerkwijk, Chang, & Justham 2010) to be a possible scenario for SN 2005ke. More spectropolarimetric observations of fast-declining SNIa will be key to determine their explosion mechanism.

All SNe in the *SN Ia-faint* subgroup are spectroscopically 91bg-like (see Table 1), however three SNe not in this subgroup are also classified as 91bg-like since they show strong Ti II in their maximum light spectra (Folatelli et al. 2013). Therefore, the presence of spectroscopic 91bg-like features is not an exclusive hallmark of the *SN Ia-faint* subgroup, although the Ti II feature in the *SN Ia-faint* subgroup SNe is stronger than the feature in the three SNe not in this subgroup.

The *SN Ia faint* subgroup are characterised by single-peaked NIR light curves. Kasen (2006) find in their low- ^{56}Ni mass models that the NIR light curves are single peaked since the shift from doubly to singly ionized iron group elements (IGEs) that creates the second maximum occurs only ~ 20 days after explosion hence, coinciding with the primary maximum. Objects in our *SN Ia-faint* subgroup have inferred ^{56}Ni masses $\lesssim 0.1 M_{\odot}$ indicating that their different NIR light curve morphology is a direct result of the low ^{56}Ni yield. We note that other fast-declining SNe, e.g. 1991bg, 1998de, show no *i*-band second maximum (Filippenko et al. 1992; Turatto et al. 1996; Modjaz et al. 2001) and a late *i*-band peak (similar to the NIR properties of the *SN Ia-faint* subgroup) which would also make them members of this subclass.

Type Iax supernovae (Foley et al. 2013) also show a single NIR maximum despite displaying a large range of decline rates ($1.2 < \Delta m_{15}(B) < 2.4$) and inferred ^{56}Ni masses ($\sim 0.001 - 0.18 M_{\odot}$). This is understood as a result of a high degree of mixing of ^{56}Ni (seen in 3-D deflagration models; e.g. Kromer et al. 2013; Fink et al. 2014) in the ejected material and is observationally supported by the rapid rise of the light curve to maximum (see for e.g. Yamanaka et al. 2015) and the presence of iron in early time spectra (for e.g. Li et al. 2003). The nebular phase spectra of SNIax, which, in some cases show P-Cygni line profiles, unlike the forbidden iron lines in nebular spectra of SNIa (e.g. Jha et al. 2006; Foley et al. 2016), along with the peculiar maximum light spectroscopic and photometric properties would point towards them being distinct explosions from the fast-declining SNe analysed here.

Pure deflagrations which only partially unbind the progenitor, leaving a bound remnant (e.g. Kromer et al. 2013; Fink et al. 2014) can explain the low M_{ej} of the *SN Ia-faint* subgroup, though the corresponding ^{56}Ni masses are higher than the values inferred from observations (Table 4). Pure deflagration models with a significantly lower M_{ej} ($\sim 0.2 M_{\odot}$) agree well with the *B*-band and bolometric light curves of *SN Ia-faint* subgroup member SN 2005bl (Taubenberger et al. 2008; Fink et al. 2014), but cannot explain the extremely red colours for these SNe. We note, however, this explosion mechanism would not be a viable

candidate for fast-decliners with two NIR maxima (e.g. SN 2007on) since the ^{56}Ni is highly mixed in the ejecta, producing theoretical light curves with only a single maximum in the NIR.

We have shown that SNIa that exhibit s_{BV} below 0.5 deviate from the $L_{\text{max}} - s_{BV}$ relation for normal SNIa, show a low NIR peak luminosity, late NIR maxima and also lack a prominent second maximum in the NIR filters. This behaviour distinguishes them from fast-declining SNIa with s_{BV} above 0.5 which seem to extend the normal SNIa sequence to fainter magnitudes. From this work it is evident that the s_{BV} metric of Burns et al. (2014) is a powerful diagnostic of the nature of the explosion. From the low bolometric luminosity we infer small ^{56}Ni mass and from fitting an energy deposition function to the tail of the bolometric light curve, we infer a sub- M_{Ch} ejecta mass. The low values for these global parameters, combined with the differences in the NIR and bolometric properties of the two subgroups of fast-declining SNIa could point to two different explosion scenarios leading to fast-declining SNIa.

References

- Ajhar E. A., Tonry J. L., Blakeslee J. P., Riess A. G., Schmidt B. P., 2001, *ApJ*, 559, 584
 Arnett W. D., 1982, *ApJ*, 253, 785
 Arnett W. D., Branch, D., Wheeler, J. C., 1985, *Nature*, 314, 337
 Benetti S., et al., 2004, *MNRAS*, 348, 261
 Bildsten, L., Shen, K. J., Weinberg, N. N., & Nelemans, G. 2007, *ApJ*, 662, L95
 Blondin S., et al., 2012, *AJ*, 143, 126
 Blondin S., Dessart L., Hillier D. J., Khokhlov A. M., 2013, *MNRAS*, 429, 2127
 Blondin S., Dessart L., Hillier D. J., 2015, *MNRAS*, 448, 2766
 Blondin S., et al., 2016, *MNRAS*, submitted
 Blondin S., 2015, *sf2a.conf*, 319
 Branch D., 1992, *ApJ*, 392, 35
 Burns C. R., et al., 2011, *AJ*, 141, 19
 Burns C. R., et al., 2014, *ApJ*, 789, 32
 Contardo G., Leibundgut B., Vacca W. D., 2000, *A&A*, 359, 876
 Contreras C., et al., 2010, *AJ*, 139, 519
 Dhawan S., Leibundgut B., Spyromilio J., Maguire K., 2015, *MNRAS*, 448, 1345
 Dhawan, S., Leibundgut, B., Spyromilio, J., & Blondin, S. 2016, *A&A*, 588, A84
 Elias, J. H., Frogel, J. A., Hackwell, J. A., Persson, E. E., 1981, *ApJ*, 251, L13
 Feroz F., Hobson M. P., Cameron E., Pettitt A. N., 2013, *arXiv*, arXiv:1306.2144
 Filippenko A. V., et al., 1992, *AJ*, 104, 1543
 Filippenko A. V., et al., 1992, *ApJ*, 384, L15
 Fink M., Röpke F. K., Hillebrandt W., Seitenzahl I. R., Sim S. A., Kromer M., 2010, *A&A*, 514, A53
 Fink M., et al., 2014, *MNRAS*, 438, 1762
 Folatelli G., et al., 2010, *AJ*, 139, 120
 Folatelli G., et al., 2013, *ApJ*, 773, 53
 Foley, R. J., et al., *AJ*, 138, 376
 Fransson, C., Jerkstrand, A., 2015, *ApJ*, 814, L2
 Freedman W. L., et al., 2001, *ApJ*, 553, 47
 Friedman A. S., et al., 2015, *ApJS*, 220, 9
 Foley R. J., et al., 2013, *ApJ*, 767, 57
 Foley R. J., Jha S. W., Pan Y.-C., Zheng W. K., Bildsten L., Filippenko A. V., Kasen D., 2016, *MNRAS*, 461, 433
 Garnavich P. M., et al., 2004, *ApJ*, 613, 1120
 Hillebrandt W., Niemeyer J. C., 2000, *ARA&A*, 38, 191
 Höflich P., Gerardy C. L., Fesen R. A., Sakai S., 2002, *ApJ*, 568, 791
 Howell D. A., 2001, *ApJ*, 554, L193
 Howell, D. A., Höflich, P., Wang, L., & Wheeler, J. C. 2001, *ApJ*, 556, 302
 Hoyle F., Fowler W. A., 1960, *ApJ*, 132, 565
 Hsiao E. Y., et al., 2015, *A&A*, 578, A9
 Jeffery D. J., 1999, *astro*, arXiv:astro-ph/9907015

- Jensen J. B., Tonry J. L., Barris B. J., Thompson R. I., Liu M. C., Rieke M. J., Ajhar E. A., Blakeslee J. P., 2003, *ApJ*, 583, 712
- Jha S., Branch D., Chornock R., Foley R. J., Li W., Swift B. J., Casebeer D., Filippenko A. V., 2006, *AJ*, 132, 189
- Kasen D., 2006, *ApJ*, 649, 939
- Kattner S., et al., 2012, *PASP*, 124, 114
- Kromer M., et al., 2013, *MNRAS*, 429, 2287
- Kromer M. et al., 2015, *MNRAS*, 450, 3035
- Krisciunas K., Phillips M.M., Suntzeff, N.B., 2004, *ApJ*, 602, 81
- Krisciunas K., et al., 2009, *AJ*, 138, 1584
- Leibundgut B., et al., 1993, *AJ*, 105, 301
- Li W., et al., 2003, *PASP*, 115, 453
- Li W., et al., 2011, *MNRAS*, 412, 1441
- Livne E., Arnett D., 1995, *ApJ*, 452, 62
- Mazzali P. A., Chugai N., Turatto M., Lucy L. B., Danziger I. J., Cappellaro E., della Valle M., Benetti S., 1997, *MNRAS*, 284, 151
- Meikle W. P. S., 2000, *MNRAS*, 314, 782
- Modjaz M., Li W., Filippenko A. V., King J. Y., Leonard D. C., Matheson T., Treffers R. R., Riess A. G., 2001, *PASP*, 113, 308
- Pakmor R., Kromer M., Röpke F. K., Sim S. A., Ruiter A. J., Hillebrandt W., 2010, *Nature*, 463, 61
- Pakmor R., Kromer M., Taubenberger S., et al., 2012, *ApJ*, 747, L10
- Patat, F., Baade, D., Höflich, P., et al. 2009, *A&A*, 508, 229
- Patat, F., Höflich, P., Baade, D., et al. 2012, *A&A*, 545, A7
- Phillips M. M., 1993, *ApJ*, 413, L105
- Phillips M. M., 2012, *PASA*, 29, 434
- Phillips M. M., Wells L. A., Suntzeff N. B., Hamuy M., Leibundgut B., Kirshner R. P., Foltz C. B., 1992, *AJ*, 103, 1632
- Phillips M. M., Lira P., Suntzeff N. B., Schommer R. A., Hamuy M., Maza J., 1999, *AJ*, 118, 1766
- Phillips, M. M., et al., 2007, *PASP*, 119, 360
- Pinto P. A., Eastman R. G., 2000, *ApJ*, 530, 757
- Scalzo R., et al., 2014, *MNRAS*, 440, 1498
- Shen K. J., Moore K., 2014, *ApJ*, 797, 46
- Sim S. A., et al., 2010, *ApJ*, 714, L52
- Ruiter A. J., Seitenzahl I. R., Skilling J., 2004, *AIPC*, 735, 395
- Stritzinger M., Leibundgut B., Walch S., Contardo G., 2006, *A&A*, 450, 241
- Stritzinger M. D., et al., 2011, *AJ*, 142, 156
- Swartz D. A., Sutherland P. G., Harkness R. P., 1995, *ApJ*, 446, 766
- Taubenberger S., et al., 2008, *MNRAS*, 385, 75
- Tomasella, L., et al., *MNRAS*, 459, 1018
- Turatto M., Benetti S., Cappellaro E., Danziger I. J., Della Valle M., Gouffes C., Mazzali P. A., Patat F., 1996, *MNRAS*, 283, 1
- Tonry J. L., Dressler A., Blakeslee J. P., Ajhar E. A., Fletcher A. B., Luppino G. A., Metzger M. R., Moore C. B., 2001, *ApJ*, 546, 681
- Trotta R., 2008, *ConPh*, 49, 71
- Tully R. B., Rizzi L., Shaya E. J., Courtois H. M., Makarov D. I., Jacobs B. A., 2009, *AJ*, 138, 323
- Tully R. B., et al., 2013, *AJ*, 146, 86
- van Kerkwijk M. H., Chang P., Justham S., 2010, *ApJ*, 722, L157
- Wang, L., Baade, D., & Patat, F. 2007, *Science*, 315, 212
- Wood-Vasey W. M., et al., 2008, *ApJ*, 689, 377
- Woosley S. E., Weaver T. A., 1994, *ApJ*, 423, 371
- Yamanaka M., et al., 2015, *ApJ*, 806, 191

Acknowledgements. This research was supported by the DFG Cluster of Excellence Origin and Structure of the Universe'. B.L. acknowledges support for this work by the Deutsche Forschungsgemeinschaft through TRR33, The Dark Universe. We all are grateful to the ESO Visitor Programme to support the visit of S. B. to Garching when this work was started. We thank Andrew Friedman for providing CfAIR2 light curves in machine-readable form and Stefan Taubenberger for discussions on rise times of fast declining SN Ia.